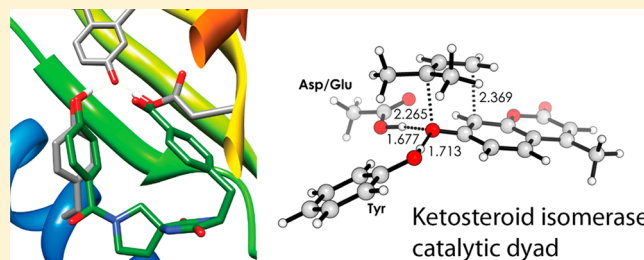


## Acceleration of an Aromatic Claisen Rearrangement via a Designed Spiroligozyme Catalyst that Mimics the Ketosteroid Isomerase Catalytic Dyad

Matthew F. L. Parker,<sup>§</sup> Silvia Osuna,<sup>‡</sup> Guillaume Bollob,<sup>‡</sup> Shivaiah Vaddypally,<sup>†</sup> Michael J. Zdilla,<sup>†</sup> K. N. Houk,<sup>‡</sup> and Christian E. Schafmeister<sup>\*,†</sup><sup>†</sup>Department of Chemistry, Temple University, 1901 North 13th Street, Philadelphia, Pennsylvania, 19122, United States<sup>‡</sup>Department of Chemistry and Biochemistry, University of California, Los Angeles, California 90095-1569, United States<sup>§</sup>Department of Chemistry, University of Pittsburgh, Pittsburgh, Pennsylvania 15260, United States

## S Supporting Information

**ABSTRACT:** A series of hydrogen-bonding catalysts have been designed for the aromatic Claisen rearrangement of a 1,1-dimethylallyl coumarin. These catalysts were designed as mimics of the two-point hydrogen-bonding interaction present in ketosteroid isomerase that has been proposed to stabilize a developing negative charge on the ether oxygen in the migration of the double bond.<sup>1</sup> Two hydrogen bond donating groups, a phenol alcohol and a carboxylic acid, were grafted onto a conformationally restrained spirocyclic scaffold, and together they enhance the rate of the Claisen rearrangement by a factor of 58 over the background reaction. Theoretical calculations correctly predict the most active catalyst and suggest that both preorganization and favorable interactions with the transition state of the reaction are responsible for the observed rate enhancement.



## 1. INTRODUCTION

One century after its discovery,<sup>2</sup> the [3,3]-sigmatropic rearrangement of allyl vinyl ethers (i.e., the Claisen rearrangement) continues to be extensively investigated and applied in the synthesis of natural products and complex organic molecules.<sup>3,4</sup> Many efforts have been devoted to develop small molecule and biocatalysts for this synthetically powerful reaction.<sup>5,6</sup> Attractive noncovalent interactions are responsible for much of the rate accelerations and stereoselectivities observed in enzyme catalysis, and active site residues can stabilize the transition state by electrostatic and noncovalent interactions.<sup>7</sup> A variety of dual hydrogen-bond donor organocatalysts such as ureas, thio-ureas, guanidinium groups, and bis-imidazoliums have been reported in the literature for Claisen rearrangements.<sup>6,8–13</sup> Some biological catalysts have also been identified,<sup>14–16</sup> and *de novo* computational design strategies for developing an aromatic Claisen biocatalyst have been carried out.<sup>17</sup> We are developing a new approach to the development of organocatalysts called “spiroligozymes” wherein we use transition state modeling to identify constellations of reactive functional groups and then build those functional groups onto a spiroligomer scaffold to see if they can act as organocatalysts.<sup>18</sup> In this manuscript, we describe the design and synthesis of a series of bis-amino acid monomers fused to amino acids through diketopiperazines, that accelerate the Claisen rearrangement of 1,1-dimethylallyl coumarin. This paper reports the successful mimicry of the catalytic dyad of bacterial

ketosteroid isomerase (KSI) in a small spiroligozyme and the catalysis of an aromatic Claisen rearrangement of a 1,1-dimethylallyl coumarin.

Aromatic Claisen rearrangements are typically performed in the temperature range of 180–225 °C,<sup>19</sup> and proceed through a concerted pericyclic pathway followed by a keto/enol tautomerization that restores aromaticity. The cyclic transition state of the Claisen rearrangement is key for understanding a number of phenomena. These include the effect of solvent on the rate of the reaction,<sup>20–27</sup> substituent effects, and stereoselectivity.<sup>4</sup> There is one well-established enzyme-catalyzed Claisen rearrangement, the chorismate to prephenate transformation catalyzed by chorismate mutase.<sup>28–33</sup> The Claisen rearrangement of O-prenylated tyrosines in a prenyltransferase from the TruF enzyme family has also been proposed,<sup>16</sup> and catalytic antibodies have been developed for the chorismate to prephenate conversion.<sup>34–36</sup>

Considerable acceleration of the Claisen rearrangement can be achieved by employing hydrogen-bonding solvents, especially water.<sup>25,26,28,37–40</sup> In 1987, Carpenter and co-workers first reported the acceleration of the Claisen rearrangement of chorismic acid and related compounds in aqueous media.<sup>28</sup> The rate of the aromatic Claisen rearrangement of allyl naphthyl ether was also increased in aqueous suspensions relative to

Received: September 5, 2013

Published: January 23, 2014

other organic solvents such as toluene, dimethylformamide, acetonitrile, and methanol.<sup>41</sup> Sharpless reported “on-water” catalysis of a Diels–Alder reaction and aromatic Claisen rearrangement. Several examples from his lab illustrated the substantial rate acceleration of the reactions when insoluble reactants were stirred in aqueous suspension. This “on water” catalysis has prompted several computational studies to unravel the origin of the rate acceleration in water and hydrogen-bonding solvents.<sup>20,21,26,28,38,42</sup> It was found that the aqueous acceleration of the Claisen rearrangement is due to a greater stabilization of the transition state by specific interactions with first shell solvent molecules.<sup>17,38,43–45</sup> Jorgensen and co-workers computationally studied the acceleration of the Claisen rearrangement in water. The model consisted of two explicit water molecules around the core heteroatom of the allyl vinyl ether.<sup>21</sup>

Curran et al. discovered that dual hydrogen-bonding catalysts such as ureas and thioureas accelerate the Claisen rearrangement and measured modest rate accelerations using NMR experiments.<sup>9</sup> In addition, protonated catalysts including those based on guanidinium,<sup>11</sup> quinolinium thioamide,<sup>46</sup> and ammonium<sup>26,47</sup> structures were also studied. The latter positively charged catalysts tend to activate electrophiles more strongly than the neutral compounds.<sup>10</sup> Jacobsen and co-workers have developed diphenylguanadinium salts as stereoselective Claisen rearrangement catalysts for a variety of substituted allyl vinyl ethers and  $\beta$ -ketoester derivatives.<sup>11,13</sup> The mechanism by which the guanidinium catalysts promote the Claisen rearrangement was also studied both experimentally and theoretically.<sup>6,12</sup> The catalysis is mainly achieved by stabilization of the developing negative charge on the oxallyl fragment, and by a secondary attractive interaction between the  $\pi$ -system of the catalyst and the partially positive allyl cation fragment.<sup>12</sup> Kozlowski and co-workers designed a bisamidinium catalyst salt able to catalyze the Claisen rearrangement through a two-point hydrogen bonding stabilization of the negatively charged ether oxygen in the transition state.<sup>8</sup>

The most prominent biological example of a Claisen rearrangement is the enzyme *Chorismate mutase*, which catalyzes the Claisen rearrangement of chorismate to prephenate more than a million-fold relative to the uncatalyzed process.<sup>15</sup> Hilvert and co-workers have also studied the enzyme catalyzed Cope rearrangement of carbachorismate to carbaprephenate in the enzyme *Bacillus subtilis* chorismate mutase (BsCM).<sup>14</sup> They showed that a positively charged residue at position 88 or 90 is essential for stabilization of the transition state of the enzymatic chorismate rearrangement.<sup>14</sup> Borden and Houk studied models for this rearrangement and tested different theozymes to determine the effect of different side chains in chorismate mutase.<sup>48</sup> Bertran et al. performed a QM/MM study where two different transition states were located for the chorismate conversion to prephenate. It was found that the enzyme stabilizes one of the transition states (TS) by means of hydrogen bonding interactions, while the other TS located, corresponded to the preferred one in vacuum and in water.<sup>49</sup> They found that aqueous solution and BsCM active site environments reduce the free energy barriers more than in the gas phase for both reactions. The catalytic effect was mainly attributed to the enhanced electrostatic stabilization of the transition state relative to the starting substrate in the Claisen rearrangement.<sup>50</sup>

Very recently, LynF, a prenyltransferase from the TruF enzyme family, was characterized.<sup>16</sup> This enzyme performs O-

prenylation of tyrosine, serine, and threonine in cyclic peptides. It was found that at physiological temperature and in aqueous buffer, O-prenylated tyrosine derivatives undergo spontaneous Claisen rearrangements.

In recent years, novel enzyme catalysts for the Kemp elimination,<sup>51</sup> retro-aldol,<sup>52</sup> and Diels–Alder<sup>53</sup> reactions have been designed, making use of the so-called “Inside-Out” approach. The first step of this protocol involves quantum mechanical calculations of the ideal arrangement of catalytic groups around the transition state of a reaction; these computed complexes are called theozymes (short for theoretical enzymes).<sup>54–56</sup> Theozymes serve as models for active site structures and for the prediction of activation barriers relative to the uncatalyzed reaction in aqueous solution. The arrangement of functional groups in the theozyme geometry is then incorporated into protein scaffolds from the Protein Data Bank<sup>57</sup> using the computational package RosettaMatch.<sup>58</sup> The active sites of the generated proteins are then minimized and repacked, and amino acids in the vicinity of the active site are mutated to stabilize the ideal transition state geometry. This process is performed using the RosettaDesign package.<sup>59,60</sup> The Inside-Out approach has been satisfactorily applied in the above-mentioned cases (Kemp elimination, retro-aldol, and Diels–Alder reaction), but it has some important limitations. Up until now, most active designed enzymes still perform quite poorly in comparison with the natural existing enzymes (i.e., natural enzymes have average  $k_{\text{cat}}/k_{\text{uncat}}$  of  $\sim 10^{11}$ , whereas artificial enzymes developed through computational modeling and directed evolution have  $k_{\text{cat}}/k_{\text{uncat}}$  values that range from  $10^2$  to  $10^5$ ).<sup>51–53,61</sup> In part, this is due to the difficulty of designing a protein with the same ideal geometry of functional groups present in the theozyme.

The design and testing of small-molecule “enzyme mimics” has been a tempting but frustrating target for organic chemists,<sup>62–66</sup> and occasional success has been reported.<sup>10,67,68</sup>

We conceived the melding of the Inside-Out approach with our recent successes in spiroligozyme syntheses to mount catalytic groups from theozymes on a spiroligomer scaffold.<sup>69</sup> Spiroligomers are shape-programmable macromolecules constructed by assembling stereochemically pure, cyclic, functionalized bis-amino acids through pairs of amide bonds to create rigidified scaffolds that present functional groups in controlled three-dimensional constellations by virtue of the sequence, shape, and stereochemistry inherent in each chiral building block.<sup>70–72</sup> Previously, spiroligomers have been utilized as catalysts for the aldol reaction and transesterification reaction.<sup>18,69</sup> We now report a combined computational and experimental approach to use spiroligozymes as catalysts for the aromatic Claisen rearrangement.

## 2. RESULTS AND DISCUSSION

**2.1. Design and Synthesis of Ketosteroid Isomerase-Inspired Catalysts for the Aromatic Claisen Rearrangement.** Bacterial ketosteroid isomerase (KSI) is heavily utilized as a model system for investigating fundamental aspects of enzyme catalysis.<sup>1,73,74</sup> Its natural function is the isomerization of the position of a double bond in steroids. The mechanism involves a general base that deprotonates the steroid forming a dienolate, which is stabilized via hydrogen bonding with a tyrosine-16 residue and a protonated aspartic acid-104 residue (see Figure 1a). The stabilized intermediate is reprotonated and the double bond isomerized. The hydrogen bonding catalytic dyad was considered a promising modality for the stabilization

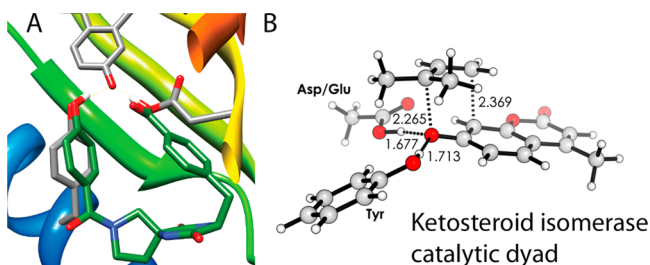


**Figure 1.** (a) Molecular model overlay of the active site of KSI (pdb code 3OWU<sup>1</sup>) with the spirologomer mimetic **BPC8**. KSI is displayed as a rainbow ribbon with Y16 and D103 shown in gray. Equilenin is bound and also shown in gray. The spirocyclic catalyst **BPC8** is displayed as dark green and is overlaid matching the oxygens of the catalytic residues. (b) The theoretical enzyme model for the KSI catalytic dyad.

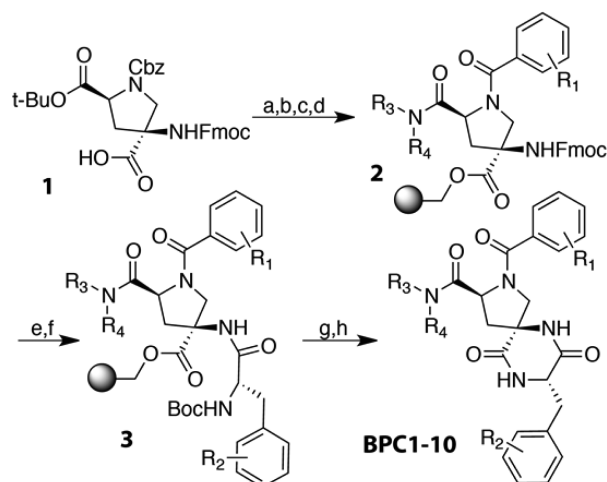
of the growing negative charge in the transition state of the Claisen rearrangement (Figure 1). It was proposed by Gerlt and Gassman that the formation of short, strong hydrogen bonds (SSHB, also called low-barrier hydrogen bonds LBHB) between the KSI oxyanion hole and the reaction intermediate stabilizes the transition state of the reaction.<sup>75,76</sup> There has been an intense debate about the role of SSHBs in enzyme catalysis.<sup>77,78</sup>

We designed a series of bioinspired spirologozyme catalysts that display a carboxylic acid and a phenol on a spirologomer backbone that resembles the hydrogen bonding catalytic dyad of KSI (see Figure 1b). The use of a phenol and carboxylic acid is a stark departure from the currently utilized organocatalysts for the Claisen rearrangement, which generally rely on N–H hydrogen-bond donors. The optimized theozyme for the aromatic Claisen rearrangement using the KSI catalytic dyad (i.e., Asp/Tyr; see Figure 1b) suggests that a 10<sup>5</sup>-fold acceleration with respect to the background reaction could be achieved (at M06-2X/6-311+G(d,p)//M06-2X/6-31G(d) and in CPCM implicit solvation for CH<sub>2</sub>Cl<sub>2</sub> with  $\epsilon = 4$ ).

Selection of the scaffold to tether the catalytic residues was accomplished by matching carboxylic acid/phenol functionalized Amber 94<sup>79</sup> minimized spirologomer structural motifs that we have synthetic access to against the crystal structure data for KIS as shown in Figure 1a (pdb code 3OWU).<sup>1</sup> A scaffold previously used for studying electron transfer in water was selected as a starting point for further optimization.<sup>80</sup> The scaffold features a single bis-amino acid building block with one functional group introduced via a 2,5-dioxopiperazine (DKP) ring and the other introduced via amide linkage at the pyrrolidine nitrogen forming a well-defined cleft between the two catalytic residues.

A series of molecules of this scaffold type were synthesized using solid phase synthesis on HMBA resin (Scheme 1).<sup>81</sup> The bis-amino acid<sup>82</sup> **1** was attached to HMBA resin with MSNT and NMI in DCM. The benzyl carbamate and *tert*-butyl ester were then removed by treatment with 33% HBr in AcOH as a 1:1 volumetric mixture with DCM. This treatment causes acetylation of all remaining hydroxyl groups on the resin. The benzoic acid derivative was introduced using HATU and DIPEA in NMP. The C-2 carboxylic acid was converted to an amide using PyAOP and the amine R<sub>3</sub>R<sub>4</sub>NH in NMP to form the resin bound intermediate **2**. The Fmoc group was removed using a 20% solution of piperidine in DMF. The phenylalanine derivative was then introduced using HATU and DIPEA in NMP to produce intermediate **3**. The *tert*-butyl carbamate,

**Scheme 1. Synthetic Scheme for the Solid Phase Assembly of Claisen Catalysts BPC1–10**



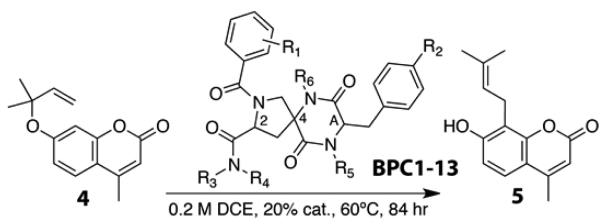
(a) HMBA Resin (1.1 equiv), MSNT (2 equiv), NMI (2 equiv), DCM (0.1 M); (b) 33% HBr in AcOH/DCM (1:1, 0.1 M); (c) Benzoic Acid derivative (3 equiv), HATU (3 equiv), DIPEA (6 equiv), NMP (0.2 M); (d) Substituted Amine (6 equiv), PyAOP (3 equiv), NMP (0.2 M); (e) 20% Piperidine in DMF (0.1 M); (f) N-Boc-Amino Acid (3 equiv), HATU (3 equiv), DIPEA (6 equiv), NMP (0.2 M); (g) TFA/DCM (1:1, 0.1 M); (h) 10% DIPEA in MeCN (0.05 M).

ester, and ether were removed with treatment with a 1:1 volumetric mixture of TFA and DCM. The DKP was closed and subsequent cleavage from the resin was affected with a 10% solution of DIPEA in MeCN. Purification with C<sub>18</sub> reverse phase HPLC yielded the pure catalysts **BPC1–10** in 60–70% isolated yields (Table 1).

The series of catalysts **BPC1–10** and controls were tested for acceleration of the aromatic Claisen rearrangement of the 1,1-dimethylallyl coumarin substrate **4**. Catalyst was added at 20 mol % relative to the substrate **4** at 0.2 M in dichloroethane. The reaction vessels were sealed and stirred magnetically at 60 °C for 84 h. High-density polypropylene vessels had to be used because untreated glass vessels lead to decomposition of the reagent, presumably catalyzed by trace acid. The reactions were analyzed by HPLC-MS. Percent conversions were obtained by comparison of the area contributions from the product **5** and starting material peaks. Rate constants were determined by fitting the concentration of product with respect to time using a first-order kinetics model. Table 1 lists relative rate constants for the catalysts as well as benzoic acid and diphenylguanidium BARF catalyst.<sup>11</sup>

The compound **BPC1** displayed a 11-fold rate enhancement relative to the background reaction (entries 1–2). **BPC1** was designed to display a terephthalic acid and a tyrosine in order to project a carboxylic acid and a phenol alcohol toward each other. Molecular modeling suggested that this would direct the terephthalic acid and phenol toward each other so that they could both simultaneously act as hydrogen bond donors to a single ether oxygen atom. This close approach of these two hydrogen-bonding groups is promoted by the stereochemistry of the spirofused pyrrolidine and diketopiperazine ring onto which the groups are mounted (Figure 1a). This close approach is analogous to the close approach that is achieved when a pyrene and a *para*-dimethylaniline group are displayed in place of the terephthalic acid and phenol.<sup>80</sup> The C-2 amide was modified to primary and tertiary amides (entries 3 and 4) to



Table 1. Kinetic Data for the Aromatic Claisen Rearrangement of **4** to **5**


entry	catalyst	C-2	C-4	A	R <sub>1</sub>	R <sub>2</sub>	R <sub>3</sub> /R <sub>4</sub>	R <sub>5</sub>	R <sub>6</sub>	k <sub>rel</sub>
1	none	-	-	-	-	-	-	-	-	1
2	BPC1	S	S	S	4-COOH	OH	iBu/H	H	H	11
3	BPC2	S	S	S	4-COOH	OH	H/H	H	H	10
4	BPC3	S	S	S	4-COOH	OH	iBu/iBu	H	H	10
5	BPC4	S	S	R	4-COOH	OH	iBu/H	H	H	2
6	BPC5	S	S	S	4-COOH	H	iBu/H	H	H	2
7	PhCOOH	-	-	-	-	-	-	-	-	2
8	BPC6	S	S	S	3-COOH	OH	iBu/H	H	H	8
9	BPC7	S	S	S	2-COOH	OH	iBu/H	H	H	4
10	BPC8	S	S	S	4-OH	COOH	iBu/H	H	H	30
11	BPC9	S	S	S	3-OH	COOH	iBu/H	H	H	6
12	BPC10	S	S	S	2-OH	COOH	iBu/H	H	H	4
13	DPGB*	-	-	-	-	-	-	-	-	14
14	BPC11	S	S	S	4-OH	COOH	iBu/H	H	Bn	42
15	BPC12	S	S	S	4-OH	COOH	iBu/H	Bn	H	40
16	BPC13	S	S	S	4-OH	COOH	iBu/H	Bn	Bn	58

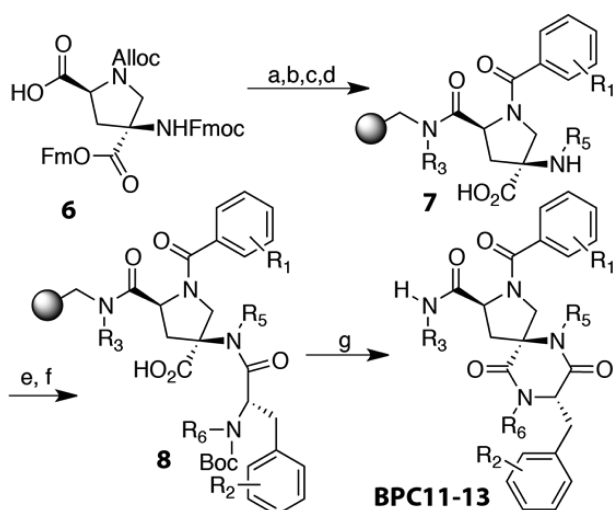
create the catalysts **BPC2** and **BPC3** which are more soluble in dichloroethane, and this does not effect the catalytic rate, suggesting that the C2 amide is not involved in hydrogen bond stabilization of the transition state. The cooperativity of the two hydrogen bond donor groups was probed by altering the stereochemistry of the bicyclic backbone to create **BPC4**, which modeling suggests would pull the two donors away from each other (entry 5)—and the activity of **BPC4** drops to 2-fold above background, which is similar to the activity of benzoic acid alone (entry 7). The cooperativity was further probed by removing the phenol alcohol using phenylalanine in place of tyrosine to form **BPC5** (entry 6) and its activity is equivalent to **BPC4** and benzoic acid. Altering the substitution of the carboxylic acid on the benzoic acid derivative to meta (**BPC6**) and ortho (**BPC7**) leads to less well-aligned hydrogen bond donor groups by modeling and leads to lower activity catalysts (entries 8 and 9). Swapping the positions of the alcohol and the carboxylic acid (**BPC8**) brings the carboxylic acid and phenol alcohol in better alignment to simultaneously donate two hydrogen bonds to a single oxygen and increased the relative rate to 30-fold over background (entry 10). Altering the position of the alcohol on the benzoic acid derivative to meta (**BPC9**) and ortho (**BPC10**) also leads to less-well-aligned hydrogen bond donor groups by modeling and led to less active catalysts (entries 11 and 12). Diphenyl guanidinium BARF (DPGB; entry 13) is a prototype of a series of asymmetric catalysts of the Claisen rearrangement developed by the Jacobsen group.<sup>11</sup> Under these reaction conditions, DPGB generated the product **5** with a  $k_{rel}$  of 14; however, concomitant with product formation, significant amounts of side products were formed, as observed by analytical reverse phase C<sub>18</sub> HPLC analysis during the course of the reaction. Among these side products, the free coumarin was observed, indicating that the guanidinium catalyst is effective, under these reaction

conditions, at breaking the ether linkage between the coumarin oxygen and allylic carbon, possibly by acting as a Bronsted acid.

Modeling suggests that the diketopiperazine ring of the BPC scaffold exists in a boat-like conformation. The boat conformation and the rotamer preferences of the functional groups could be altered through N-alkylation of the amide nitrogens within the diketopiperazine ring, and this could alter the presentation of the phenol and carboxylic acid groups and change their catalytic activity. Dichloroethane solutions of **BPC1–10** are cloudy at room temperature, although clear at 60 °C, which we attributed to diketopiperazine-tape formation at room temperature.<sup>83</sup> N-Alkylation could also improve the solubility of the catalysts in the dichloroethane solvent because it would disrupt hydrogen-bonded tape-formation. We created three N-alkylated versions of **BPC8**, the mono N-benzylated catalysts **BPC11** and **BPC12**, and the di-N-benzylated catalyst **BPC13**. Unlike **BPC1–10**, these new catalysts were completely soluble in dichloroethane at 40 mM at room temperature, as well as at 60 °C, under the reaction conditions.

In order to synthesize these, an alternative solid phase synthesis had to be devised to assemble the tetra- and penta-substituted DKP rings shown in Scheme 2. The bis-amino acid derivative<sup>82</sup> **6** was attached to an isobutyl amine modified formyl resin via HATU promoted acylation. The pyrrolidine Alloc group was removed using palladium catalyst in the presence of a scavenger and then acylated with the *t*-butyl-protected 4-hydroxy benzoic acid. The C-4 amino acid protecting group was then removed followed by reductive alkylation to the C-4 nitrogen with benzaldehyde to form **7**. The carboxy-phenylalanine derivative was introduced via HATU promoted acylation. Treatment of the resin with neat TFA was used to cleave the intermediate from the resin, which led to spontaneous diketopiperazine formation and concomitant removal of all protecting groups. Purification with reverse

Scheme 2. Synthetic Scheme for the Solid Phase Assembly of Spiroligomer Claisen Catalysts BPC11–13



(a) Substituted Amino Resin (1 equiv), HATU (1 equiv), DIPEA (2 equiv), NMP (0.2 M); (b)  $(\text{P}(\text{Ph})_3)_4\text{Pd}(0)$  (0.3 equiv),  $\text{BH}_3\cdot\text{DMA}$  (6 equiv), DCM (0.1 M); (c) Benzoic Acid Derivative (3 equiv), HATU (3 equiv), DIPEA (6 equiv), NMP (0.2 M); (d) 20% Piperidine in DMF (0.1 M); (e) PhCHO (2 equiv);  $\text{NaH}_3\text{BCN}$  (2 equiv); DMF (0.1 M); (f) Boc-Amino Acid (3 equiv); HATU (3 equiv), DIPEA (6 equiv); NMP (0.2 M); (g) TFA.

phase HPLC yielded the pure catalysts in 75–80% yields relative to solid support loading.

Kinetic studies of catalysts BPC1, BPC8, and BPC11–13 are shown in Figure 2. Improvement in catalytic rate was observed

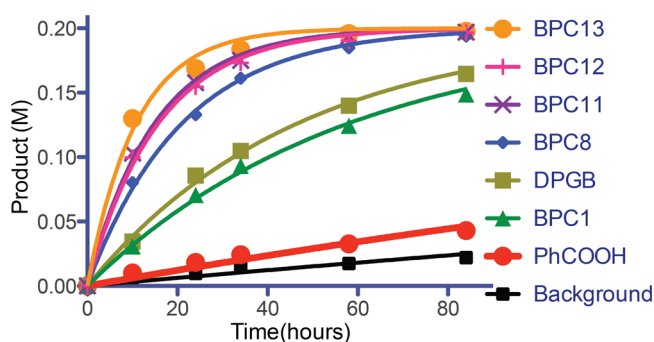


**Figure 2.** Claisen rearrangement product formation as a function of time and catalyst (0.2 M substrate in dichloroethane, 60 °C, 0.02 M catalyst).

over the course of each catalyst generation with BPC13 ( $k_{\text{rel}} = 58$ ) providing the largest rate enhancement relative to the background reaction.

The catalyst BPC1 was crystallized from water/acetonitrile 1:1 at room temperature and its crystal structure was determined (Figure 3). In the crystal structure the tyrosine side chain is observed to fold back over the diketopiperazine and pyrrolidine rings in the conformation that was proposed for dual hydrogen bonded catalysis. The terephthalic acid is rotated away from the tyrosine in one of the two available amide rotamers. The preference of this rotamer of the terephthalic acid in the crystal structure can be understood in terms of crystal packing forces and an intermolecular hydrogen bond between the amide carbonyl of the terephthalic acid and the

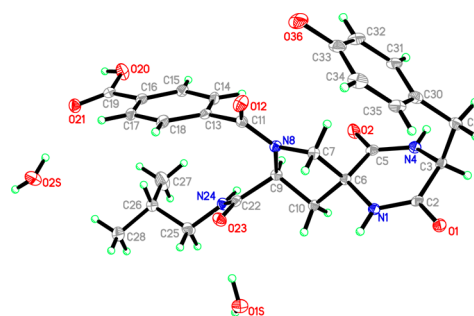


**Figure 3.** X-ray crystal structure of BPC1 illustrates the proposed catalytically active conformation of the tyrosine side chain and one of the two possible amide rotamers of the terephthalic acid. This X-ray observed conformation is very similar to BPC1a (Figure 4b), one of the lowest energy predicted structures of BPC1.

tyrosine alcohol of another molecule of BPC1. The X-ray crystal structure is very similar to the predicted conformation BPC1a in Figure 4b.

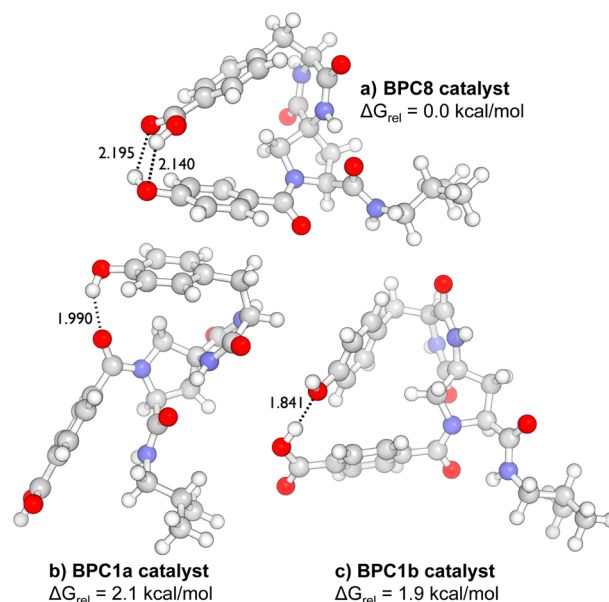


**Figure 4.** M06-2X/6-31G(d) optimized structures for the lowest energy conformers for BPC8, BPC1a, and BPC1b. M06-2X/6-311+G(d,p)/M06-2X/6-31G(d) relative Gibbs free energies have been computed using the thermal corrections at M06-2X/6-31G(d) level ( $\Delta G_{\text{rel}}$  are relative to BPC8(a) which can be calculated given that BPC1 and BPC8 have the same number of atoms, all distances are represented in Å).

**2.2. Quantum Mechanical and Molecular Dynamics Evaluation of the Catalysts.** We have explored the catalysis by BPC1, BPC8, and BPC11–13 using molecular dynamics (MD) to explore the conformational space of each catalyst and used quantum mechanics (QM) to evaluate transition states. We performed a conformational analysis of BPC1, BPC8, and BPC11–13 using the Monte Carlo (MCM) method and the OPLS-AA force field as implemented in the MacroModel computational package (see SI for a detailed description of the computational methods used).<sup>84,85</sup> In each case, 20 or more lower energy conformers were further reoptimized using the hybrid meta exchange-correlation DFT functional M06-2X,<sup>86</sup> which includes medium-range correlation, with the standard 6-

31G(d) basis set.<sup>87,88</sup> Solvent effects were included with the conductor-like polarizable continuum model (CPCM)<sup>89</sup> with dichloroethane as the solvent. M06-2X/6-31G(d) energies indicated that the lowest energy conformer for **BPC8** is from 6.5 up to 18.6 kcal/mol more stable than the rest of the computed conformers. The situation for **BPC1** is slightly different as the lowest energy conformer (**BPC1a**) is only 0.2 kcal/mol more stable than **BPC1b**, with the rest of the computed conformers being from 4 up to 15 kcal/mol higher in energy (see Figure 4). **BPC8** and **BPC1b** both present close approaching, preorganized carboxylic acid and phenol groups for catalysis, while **BPC1a** has these two functional groups far separated (see Figure 4).

The optimized transition state structures with catalytic conformations of **BPC8**, **BPC1a**, and **BPC1b** are shown in Figure 6. The computed activation barrier for the Claisen rearrangement catalyzed by **BPC8** is 28.1 kcal/mol with respect to isolated reactants (i.e., **BPC8** and the coumarin reactant). As a reference, the computed activation barrier in terms of free Gibbs energy for the background reaction is 30.0 kcal/mol at the M06-2X/6-311+G(d,p)//M06-2X/6-31G(d) level of theory in CPCM dichloroethane (see Figure 5). The catalyzed

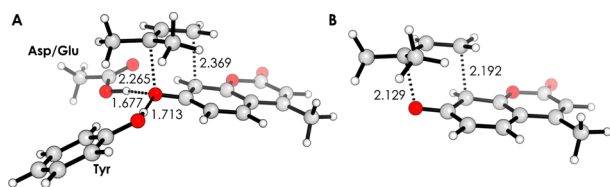


**Figure 5.** M06-2X/6-31G(d) optimized structures for the (a) theozyme with the Asp/Glu and Tyr motif and (b) the uncatalyzed reaction (all distances are represented in Å).

reaction is bimolecular, and the rate of rearrangement is considerably faster than the background, but there is unfavorable entropy of association of the substrate and catalyst. The reactant complex between **BPC8** and the 1,1-dimethylallyl coumarin ether is 3.9 kcal/mol higher in Gibbs free energy than isolated reactants; that is, the nearly 10 kcal/mol binding is counteracted by  $-T\Delta S$  for the bimolecular association. In the transition state, both hydroxyl groups of **BPC8** are stabilizing the partial negative charge on the ether oxygen and are approximately 1.7 Å away (see Figure 6). The breaking O–C and the forming C–C bond distances are 2.274 and 2.416 Å, respectively. For **BPC1a**, the catalysis of the aromatic Claisen rearrangement could be assessed considering two different approaches. The phenol group and the benzoic acid moiety are not in close contact. Instead, the hydroxyl group of the phenol is interacting with a carbonyl group of the bis-peptide backbone (see Figures 4b and 6b). Therefore, the **BPC1a** catalyzed reaction was studied using either the phenol or the carboxylic group individually hydrogen bonded to the ether oxygen of the coumarin transition state. A lower energy transition state was found for the phenol-mediated catalysis. This single hydrogen-bonding TS has a computed Gibbs free activation barrier of 30.9 kcal/mol relative to isolated reactants, **BPC1a** and the coumarin ether. At the TS, the hydrogen bond distance between the ether oxygen and the hydrogen of the phenol is 1.743 Å, and the C–O breaking and C–C forming bond are 2.159 and 2.279 Å, respectively. The coumarin analogue is nicely  $\pi$ -stacked to the benzoic acid moiety (the distance between the center of mass of the benzene rings is

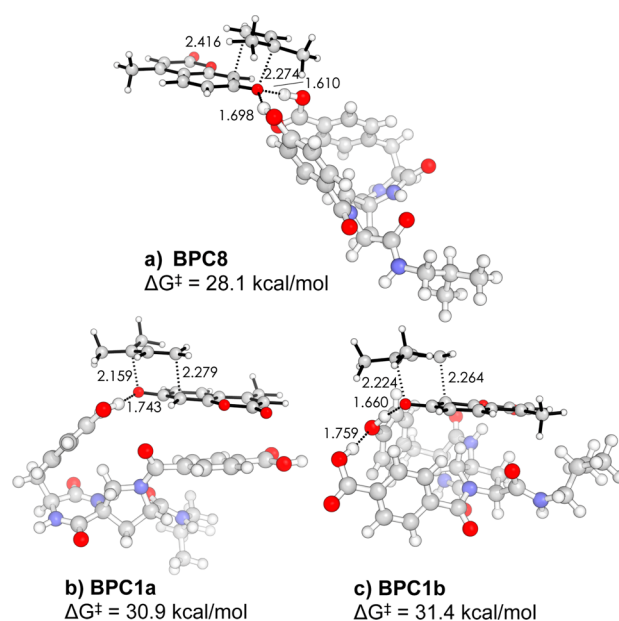


**Figure 6.** M06-2X/6-311+G(d,p)//M06-2X/6-31G(d) optimized transition state structures for the Claisen rearrangement catalyzed by (a) **BPC8**, (b) **BPC1a**, and (c) **BPC1b** in dichloroethane using CPCM implicit solvation model. The uncatalyzed reaction has a Gibbs free activation barrier of 30.0 kcal/mol. All distances are represented in Å.

approximately 3.3 Å). An enantiomer bound to the same catalyst was also found, but was 0.2 kcal/mol higher in energy. The transition state involving **BPC1b**, which has both hydroxyl groups in a closer disposition, presents an activation barrier that is 0.5 kcal/mol higher than the previous TS for **BPC1a** (the Gibbs free activation barrier compared to isolated reactants is 31.4 kcal/mol; see Figure 6c). This slightly higher activation barrier is mainly attributed to the fact that only the hydroxyl group of the phenol moiety is stabilizing the negative charge of the ether oxygen, and more importantly the favorable  $\pi$ -stacking interaction between the coumarin derivative and the benzoic acid moiety is lost (see Figure 6c). In both **BPC1a** and **BPC1b** cases, the computed Gibbs activation barriers are slightly larger than background reaction.

We have also studied the more active catalysts **BPC11**–**13**. The conformational analysis and the subsequent optimization at M06-2X/6-31G(d) level indicated that the lowest energy conformers for all three cases present the proper arrangement for catalysis with the carboxyl and the phenol group in close proximity (see Figure 7, Figure S1 and SI for more details).

We have studied the spiroligozone catalyzed Claisen rearrangement of the lowest energy conformers of the catalysts (i.e., 4 for **BPC11**, 4 for **BPC12**, and 4 for **BPC13**). It should be emphasized here that the main differences between the 4 different conformers studied for each case arise mainly from different conformations of the benzyl and isopropyl substituents (see Figure S1). The difference in energy between the different conformers is less than 4 kcal/mol in all cases. We calculated the energy of each catalyst bound to the substrate relative to the energy of the lowest energy conformer of each unbound catalyst and substrate. The energies are 8.7, 6.9, and 5.2 kcal/mol for **BPC11**, **BPC12**, and **BPC13**, respectively (see Figure S2). For **BPC11** the OH hydrogen bond (2.2 Å) is substantially longer than for the other two cases (1.85 Å). The OH in **BPC11** is also hydrogen bonded to the CO of the



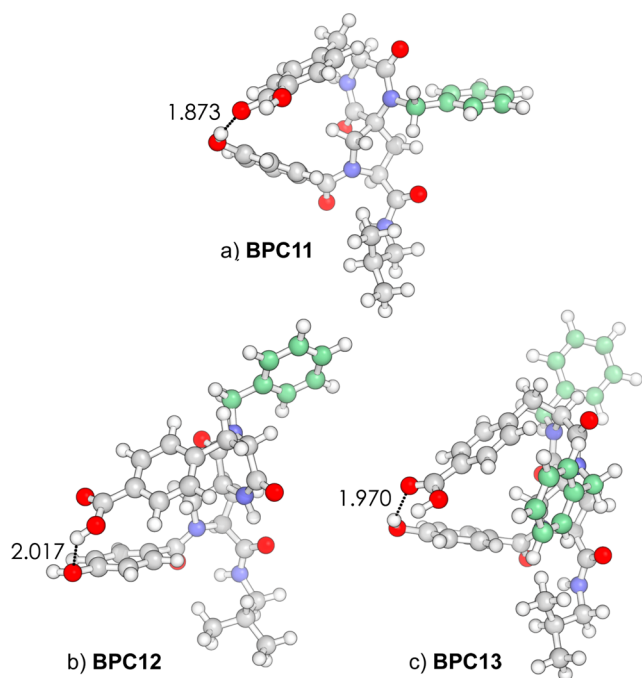


**Figure 7.** M06-2X/6-31G(d) optimized structures for the lowest energy conformers for (a) **BPC11**, (b) **BPC12**, and (c) **BPC13**. The benzyl substituents have been marked in light green for clarity. All distances are represented in Å.

carboxylic moiety (2.1 Å). The hydrogen bond length for COOH to the substrate is progressively decreased from **BPC11** to **BPC13**. **BPC13** has similar hydrogen bond lengths for both OH and COOH, so the reactant complex for **BPC13** presents a closer arrangement to the TS structure (Figure 10), which presents hydrogen bond distances of ca. 1.7 Å.

Molecular dynamics (MD) simulations using AMBER11<sup>90</sup> and a 10 Å truncated octahedral box with explicit chloroform molecules (see SI for further details) were performed in order to determine the relative free energies of catalytic and noncatalytic conformers of the catalyst. In Figure 8, the average distances between both oxygen atoms of the phenol and benzoic acid moieties of the spirologozymes ( $d(\text{O}_{\text{OH}}-\text{O}_{\text{OH}})$ ) along the 1  $\mu\text{s}$  MD simulation are represented. In Figure 9, the histograms for the  $\text{O}_{\text{OH}}-\text{O}_{\text{OH}}$  distance are provided. The standard deviation is also shown using a shaded area and has been computed every 20 ps. For each catalyst analyzed in this way (i.e., **BPC8** and **BPC11–13**), 250 superimposed MD snapshots have also been included where both the open and closed conformations have been marked using two different colors. The ideal arrangement for catalysis is substantially altered along the simulation for **BPC8**, **BPC11**, and **BPC13** catalysts (see Figures 8 and 10). The distance between the hydroxyl groups of both the phenol and benzoic acid moieties ( $d(\text{O}_{\text{OH}}-\text{O}_{\text{OH}})$ ) along the MD trajectory for **BPC8** and **BPC11–13** are  $5.86 \pm 2.87$ ,  $5.16 \pm 2.61$ ,  $4.39 \pm 0.88$ , and  $4.68 \pm 1.80$  Å, respectively. These distances are substantially longer than the optimized QM value of 2.84 Å, especially for **BPC8** and **BPC11** cases. The higher distance and deviation found for **BPC8** and **BPC11** is due to a conformational change that leads to an arrangement where both benzoic acid and phenol moieties are not interacting (see snapshots in Figure 8, and histograms in Figure 9). Interestingly, in most cases more than 100 ns of simulation is needed to observe the latter

conformational change (see plots in Figure 8). MD simulations indicate that the correct arrangement for catalysis is present 68.5% of the simulation time for **BPC8**. In this suitable arrangement, the averaged  $\text{O}_{\text{OH}}-\text{O}_{\text{OH}}$  distance is  $4.41 \pm 0.79$  Å, which is still substantially longer than the QM value of 2.84 Å. The distance between hydroxyl groups is less than 4 Å 14.5% of the simulation time. The introduction of a benzyl substituent on the amide backbone leads to a substantial improvement. **BPC11** adopts the proper conformation for catalysis ca. 74% of the simulation time, and the averaged  $\text{O}_{\text{OH}}-\text{O}_{\text{OH}}$  distance for this arrangement is  $3.73 \pm 0.51$  Å. The arrangement stays close to the QM value (i.e., less than 3 Å) 55.5% of the time. The benzoic acid moiety in **BPC12** stays in the proper orientation ca. 99% of the time; however, the  $\text{O}_{\text{OH}}-\text{O}_{\text{OH}}$  distance is close to the QM value 32.1% of the simulation time. **BPC13**, which has benzyl substituents on both amide backbone nitrogens, adopts the correct arrangement ca. 94% of the time during the MD trajectory. The averaged  $\text{O}_{\text{OH}}-\text{O}_{\text{OH}}$  distance for the **BPC13** suitable arrangement for catalysis is  $4.41 \pm 0.79$  Å; the  $\text{O}_{\text{OH}}-\text{O}_{\text{OH}}$  distance is less than 4 Å 31.9% of the time. The MD simulations performed on the free catalysts have shown that the ideal arrangement for catalysis is substantially modified, especially in the case of **BPC8**. In the case of **BPC11**, **BPC12**, and **BPC13**, those conformers with the suitable arrangement for catalysis present averaged  $\text{O}_{\text{OH}}-\text{O}_{\text{OH}}$  distances closer to the optimized QM value. These simulations indicate the fraction of conformers that have the catalytic groups properly preorganized for catalysis.

We have also computed the Gibbs free activation energies for the spirologozyme catalyzed Claisen rearrangement involving **BPC11**, **BPC12**, and **BPC13**. In Figure 10, the M06-2X/6-31G(d) optimized transition state structures for the lowest activation barrier with each catalyst are shown. The computed activation barriers for **BPC11**, **BPC12**, and **BPC13** are 28.8, 29.1, and 25.7 kcal/mol referred to the reactants: the isolated spirologozyme, each in their lowest energy conformer, and the coumarin ether. Minor differences are observed among the computed activation barriers, especially in the case of **BPC11** and **BPC12**. As mentioned earlier for **BPC1** and **BPC8**, the optimized reactant complexes are ca. 7–9 kcal/mol higher in Gibbs-free energy than isolated reactants in the case of **BPC11** and **BPC12**, and ca. 5 kcal/mol in **BPC13**. In all cases, the breaking O–C and the forming C–C bond distances are approximately 2.260 and 2.390 Å (see Figure 10). The hydrogen bonds formed between the ether oxygen and the phenol and benzoic acid moieties to stabilize the partial negative charge are 1.710 and 1.692, and 1.734 and 1.640 Å in **BPC11** and **BPC12**, respectively. Interestingly, **BPC13** presents slightly shorter hydrogen bond distances of 1.620 and 1.718 Å.

The computed activation barriers for the uncatalyzed and **BPC1**, **BPC8**, and **BPC11–13** catalyzed Claisen rearrangements at 333 K are 30.0, 30.9, 28.1, 28.8, 29.1, and 25.7 kcal/mol, respectively. MD simulations have shown that **BPC8** and **BPC11–13** adopt the appropriate conformation for catalysis (the hydroxyl distance is less than 4 Å) 14.5%, 55.5%, 32.1%, and 31.9% of the simulation time, respectively. The latter fraction of conformers ( $f$ ) in the catalytic conformation must be used to estimate the experimental rate constant ( $k_{\text{cat}} = f \cdot k_{\text{cat,computed}}$ ). Each value  $k_{\text{cat,computed}}$  is calculated from  $\Delta G_{\ddagger}^{\text{calculated}}$  using transition state theory. This leads to a computed  $k_{\text{cat}}/k_{\text{uncat}}$  of ca. 3 and 210 for **BPC8** and **BPC13** with respect to the background reaction, respectively. We calculated quantum

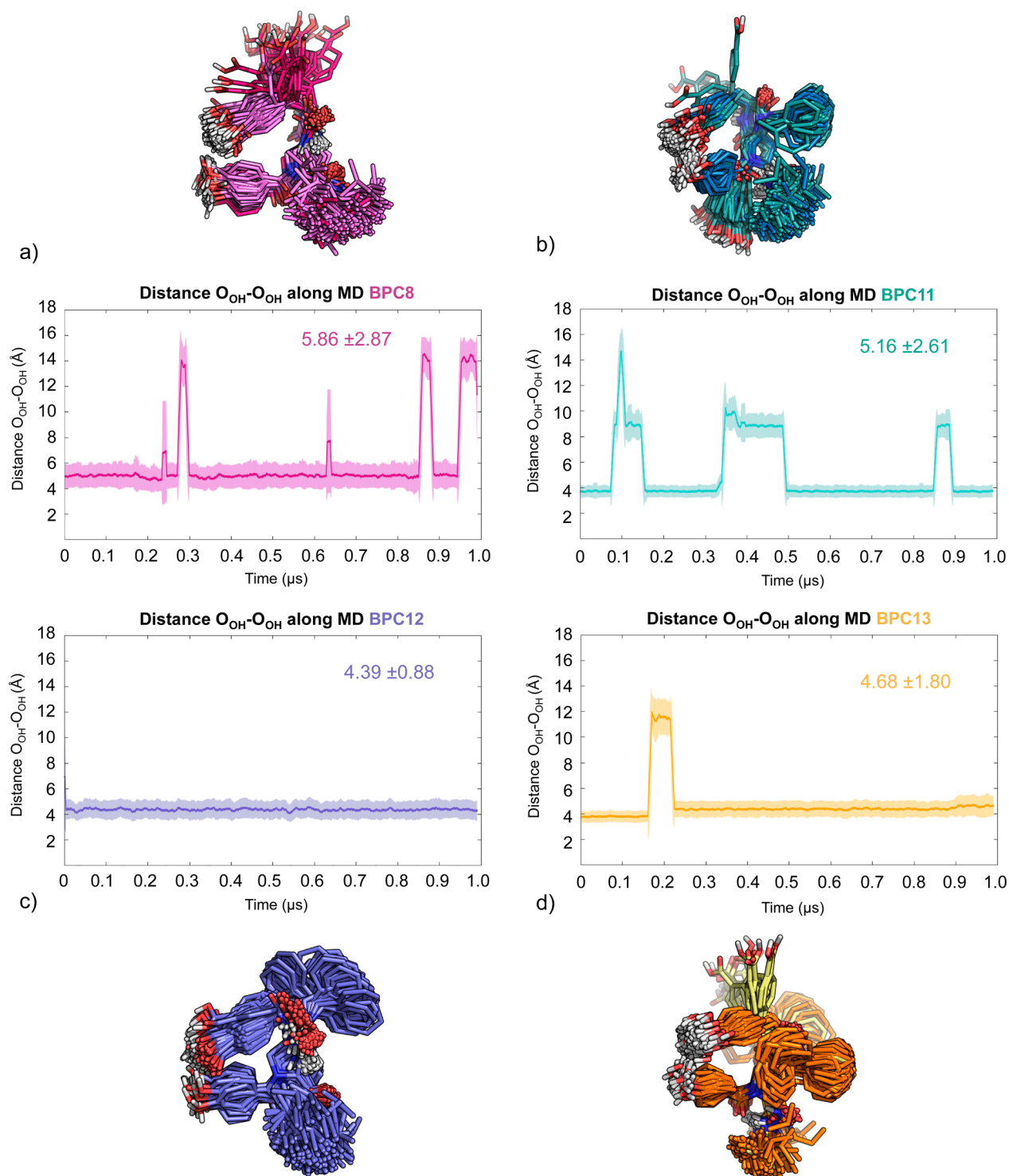


**Figure 8.** Representation of 250 superimposed MD snapshots for (a) BPC8 (magenta), (b) BPC11 (cyan), (c) BPC12 (purple), and (d) BPC13 (gold). The plots monitoring the  $\text{O}_{\text{OH}}-\text{O}_{\text{OH}}$  distance along the 1  $\mu\text{s}$  MD trajectory for these catalysts are also included. The computed QM distance at M06-2X/6-31G(d) is ca. 2.836 Å. The mean (dark line) and standard deviation of the  $\text{O}_{\text{OH}}-\text{O}_{\text{OH}}$  distance is represented using a shaded area (width is 1 std dev) and have been calculated every 10 steps of the simulation (i.e., 20 ps) (all distances are expressed in Å).

mechanical distortion energies by removing the substrate from each transition state structure and carrying out a single-point energy calculation at this geometry and subtracting the minimum energy conformation of each catalyst. The distortion energies were 6.8, 5.1, 8.8, and 3.6 kcal/mol for BPC8, BPC11, BPC12, and BPC13, respectively. The lower activation barrier

observed for BPC13 is attributed to the lower distortion energy needed to distort the catalyst to adopt the TS geometry.

Using transition state theory we calculated the  $\Delta\Delta G_{\text{expt}}^{\ddagger}$  values from the relative rate enhancements and plotted them against the  $\Delta\Delta G_{\text{calc}}^{\ddagger}$  values (Table 2). The calculations correctly predict that BCP13 will be the most active catalyst, that BPC8, BPC11, and BCP12 will have intermediate activity,



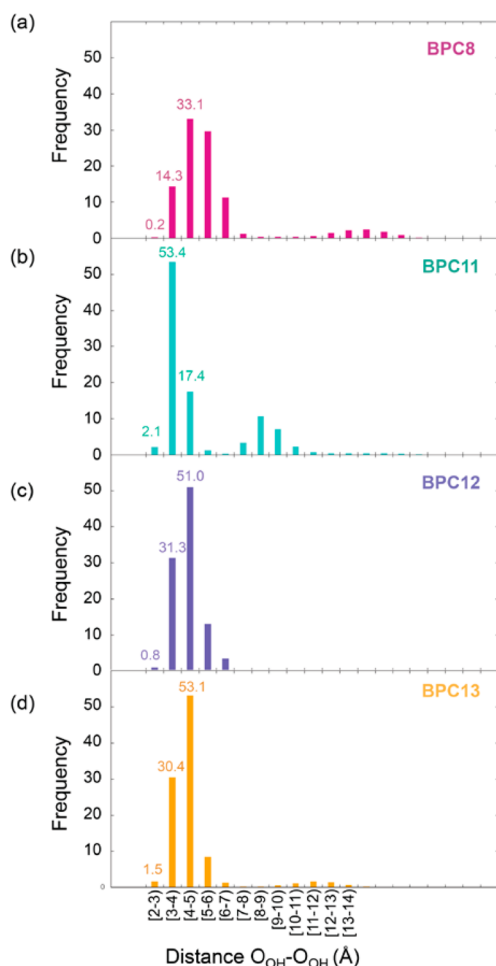


**Figure 9.** Distribution of the  $\text{O}_{\text{OH}}-\text{O}_{\text{OH}}$  distance during the 1  $\mu\text{s}$  MD trajectory for (a) **BPC8** (magenta), (b) **BPC11** (cyan), (c) **BPC12** (purple), and (d) **BPC13** (gold). All distances are expressed in Å.

and that **BPC1** will have the lowest activity. A linear fit of the two sets of values has a slope of 4.0, and so while the calculations predict the trend of activity, they predict higher activity of the catalysts than is observed. The calculations of reaction rates are based upon separated reactants in solution as the reference. Since hydrogen bonding groups, especially carboxylic acids, are known to form observable complexes with ca. 380  $\mu\text{M}$  dissociation constants in non-hydrogen-bonding solvents (carboxylic acid dimers),<sup>91</sup> the catalysts and substrates are expected to form stabilized hydrogen bonding complexes in solution, thus increasing the activation barriers as compared to the calculations reported here.

## CONCLUSIONS

We have developed a series of dual hydrogen-bond donor catalysts for the aromatic Claisen rearrangement modeled on the active site of Ketosteroid Isomerase. These catalysts are designed to present a carboxylic acid and a phenol alcohol that each simultaneously donate one hydrogen bond donor to a single ether oxygen of the 1,1-dimethylallyl coumarin substrate to stabilize the developing negative charge on the ether oxygen in the transition state of the Claisen rearrangement. The catalysts provide increasing reactivity as they better organize their hydrogen bonding groups and more closely approximate the functional group display observed in Ketosteroid Isomerase

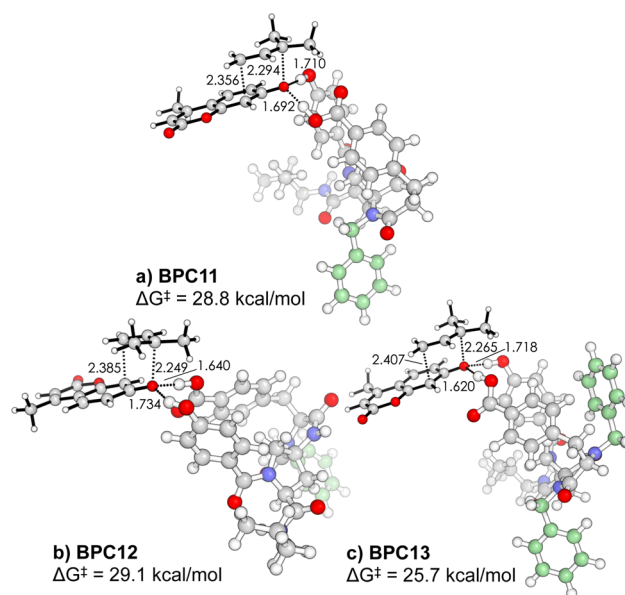
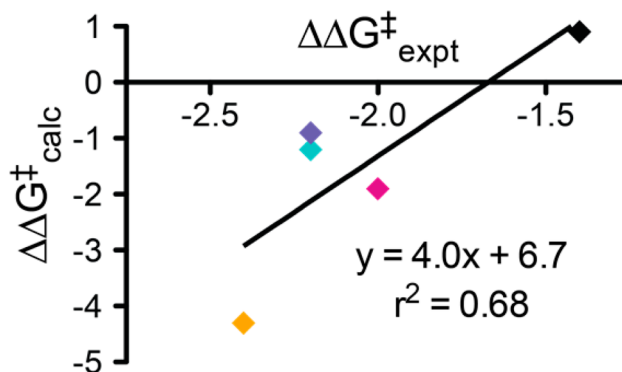


**Figure 10.** M06-2X/6-311+G(d,p)//M06-2X/6-31G(d) optimized transition state structures for the Claisen rearrangement catalyzed by (a) **BPC11**, (b) **BPC12**, and (c) **BPC13** in dichloroethane using CPCM implicit solvation model. The uncatalyzed reaction has a Gibbs free activation barrier of 30.0 kcal/mol. All distances are represented in Å.

**Table 2.** Comparison of Experimentally Derived Relative Activation Barriers to Prediction

Entry	Catalyst	$k_{\text{rel}}$	$\Delta G^\ddagger_{\text{calc}}$ <sup>a</sup>	$\Delta\Delta G^\ddagger_{\text{calc}}$	$\Delta\Delta G^\ddagger_{\text{expt}}$ <sup>b</sup>
1	none	1	30	0	0
2	<b>BPC1</b>	11	30.9	0.9	-1.4
10	<b>BPC8</b>	30	28.1	-1.9	-2
14	<b>BPC11</b>	42	28.8	-1.2	-2.2
15	<b>BPC12</b>	40	29.1	-0.9	-2.2
16	<b>BPC13</b>	58	25.7	-4.3	-2.4



<sup>a</sup>From Figures 6 and 10. <sup>b</sup>Derived using transition state theory.

and as they are better able to stabilize the transition state as determined by transition state modeling. The first designed catalyst **BPC1** accelerates the reaction 11-fold relative to background, while the best catalyst, **BPC13**, accelerates the reaction 58-fold. The combined QM and MD computational study of these systems established that **BPC13** gives a higher acceleration of the reaction due to an optimal disposition of the hydroxyl groups of both the phenol and benzoic acid moieties in both the TS and the reactant complex. This optimal

arrangement is induced by the benzyl substituents of the amide backbone, which limit the movement of the benzoic acid and phenol moieties. MD simulations have determined that this arrangement is better conserved in the case of **BPC13** and **BPC11**. The higher efficiency of **BPC13** compared to **BPC8**, **BPC11**, and **BPC12** is due to the combination of a lower activation barrier due to a lower distortion energy, and a better preorganization of **BPC13**, which maintains both hydrogen donors in close proximity ca. 94% of the time during the 1  $\mu$ s MD simulation. Comparison of the experimentally determined activation barrier lowering to calculated values demonstrates that calculations overestimate the catalytic power of the two hydrogen bond catalysis by 4-fold: this is most likely due to our lack of understanding and the difficulty modeling how solvation and self-association affect the energies of the ground states and transition states.

These catalysts represent the first examples of synthetic Claisen rearrangement catalysts that utilize O–H hydrogen bond donors as found in the Ketosteroid Isomerase enzyme rather than N–H hydrogen bond donors observed in urea-, thiourea-, guanidinium-, and bisimidazolium-based catalysts of the Claisen rearrangement.

## ■ ASSOCIATED CONTENT

### ■ Supporting Information

Synthesis of reaction substrate and **BPC1–13**, kinetic measurements, computation details, Cartesian coordinates, absolute energies, and 3D representations of all optimized structures, snapshots from molecular dynamics simulations, and crystallographic data. This material is available free of charge via the Internet at <http://pubs.acs.org>.

## ■ AUTHOR INFORMATION

### Corresponding Author

\*E-mail address: [meister@temple.edu](mailto:meister@temple.edu).

### Funding

This work was supported by the Defense Threat Reduction Agency (DOD-DTRA) (HDTRA1–09–1–0009) and we are grateful to the National Institute of General Medical Sciences, the National Institutes of Health Grant (GM-36700 and GM067866), and the Defense Advanced Research Projects Agency for additional financial support of this research.

### Notes

The authors declare no competing financial interest.

## ■ ACKNOWLEDGMENTS

This work used the Extreme Science and Engineering Discovery Environment (XSEDE), which is supported by National Science Foundation grant number OCI-1053575. S.O. acknowledges the European Community for the postdoctoral fellowship PEOF-GA-2009-252856. This research was supported by an allocation of advanced computing resources provided by the National Science Foundation (TG-CHE100059). The computations were performed on Kraken at the National Institute for Computational Sciences (<http://www.nics.tennessee.edu/>). We thank Professor David Dalton for helpful discussions regarding kinetics experiments.

## ■ REFERENCES

- (1) Fafarman, A. T.; Sigala, P. A.; Schwans, J. P.; Fenn, T. D.; Herschlag, D.; Boxer, S. G. *Proc. Natl. Acad. Sci. U.S.A.* **2012**, *109*, E299.
- (2) Claisen, L. *Chem. Ber.* **1912**, *43*, 3157.
- (3) (a) Martín Castro, A. M. *Chem. Rev.* **2004**, *104*, 2939. (b) Rehbein, J.; Hiersemann, M. *Synthesis* **2013**, *45*, 1121. (c) Kirsten, M.; Rehbein, J.; Hiersemann, M.; Strassner, T. *J. Org. Chem.* **2007**, *72*, 4001.
- (4) Ziegler, F. E. *Chem. Rev.* **1988**, *88*, 1423.
- (5) Majumdar, K. C.; Alam, S.; Chattopadhyay, B. *Tetrahedron* **2008**, *64*, 597.
- (6) Knowles, R. R.; Jacobsen, E. N. *Proc. Natl. Acad. Sci. U.S.A.* **2010**, *107*, 20678.
- (7) Warshel, A.; Sharma, P. K.; Kato, M.; Xiang, Y.; Liu, H.; Olsson, M. H. M. *Chem. Rev.* **2006**, *106*, 3210.
- (8) Annamalai, V. R.; Linton, E. C.; Kozlowski, M. C. *Org. Lett.* **2008**, *11*, 621.
- (9) Curran, D. P.; Lung, H. K. *Tetrahedron Lett.* **1995**, *36*, 6647.
- (10) Rodriguez, A. A.; Yoo, H.; Ziller, J. W.; Shea, K. J. *Tetrahedron Lett.* **2009**, *50*, 6830.
- (11) Uyeda, C.; Jacobsen, E. N. *J. Am. Chem. Soc.* **2008**, *130*, 9228.
- (12) Uyeda, C.; Jacobsen, E. N. *J. Am. Chem. Soc.* **2011**, *133*, 5062.
- (13) Uyeda, C.; Rötheli, A. R.; Jacobsen, E. N. *Angew. Chem., Int. Ed.* **2010**, *49*, 9753.
- (14) Aemissegger, A.; Jaun, B.; Hilvert, D. *J. Org. Chem.* **2002**, *67*, 6725.
- (15) Andrews, P. R.; Smith, G. D.; Young, I. G. *Biochemistry* **1973**, *12*, 3492.
- (16) McIntosh, J. A.; Donia, M. S.; Nair, S. K.; Schmidt, E. W. *J. Am. Chem. Soc.* **2011**, *133*, 13698.
- (17) Osuna, S.; Kim, S.; Bollot, G.; Houk, K. N. *Eur. J. Org. Chem.* **2013**, *2013*, 2823.
- (18) Zhao, Q.; Lam, Y. H.; Kheirabadi, M.; Xu, C.; Houk, K. N.; Schafmeister, C. E. *J. Org. Chem.* **2012**, *77*, 4784.
- (19) Claisen, L. *Chem. Ber.* **1912**, *43*, 3157.
- (20) Cramer, C. J.; Truhlar, D. G. *J. Am. Chem. Soc.* **1992**, *114*, 8794.
- (21) Severance, D. L.; Jorgensen, W. L. *J. Am. Chem. Soc.* **1992**, *114*, 10966.
- (22) White, W. N.; Wolfarth, E. F. *J. Org. Chem.* **1970**, *35*, 2196.
- (23) Coates, R. M.; Rogers, B. D.; Hobbs, S. J.; Curran, D. P.; Peck, D. R. *J. Am. Chem. Soc.* **1987**, *109*, 1160.
- (24) Grieco, P. A.; Brandes, E. B.; McCann, S.; Clark, J. D. *J. Org. Chem.* **1989**, *54*, 5849.
- (25) Brandes, E.; Grieco, P. A.; Gajewski, J. J. *J. Org. Chem.* **1989**, *54*, 515.
- (26) Gajewski, J. J. *Acc. Chem. Res.* **1997**, *30*, 219.
- (27) Sehgal, A.; Shao, L.; Gao, J. *J. Am. Chem. Soc.* **1995**, *117*, 11337.
- (28) Gajewski, J. J.; Jurayj, J.; Kimbrough, D. R.; Gande, M. E.; Ganem, B.; Carpenter, B. K. *J. Am. Chem. Soc.* **1987**, *109*, 1170.
- (29) Pawlak, J. L.; Padykula, R. E.; Kronis, J. D.; Aleksejczyk, R. A.; Berchtold, G. A. *J. Am. Chem. Soc.* **1989**, *111*, 3374.
- (30) Guilford, W. J.; Copley, S. D.; Knowles, J. R. *J. Am. Chem. Soc.* **1987**, *109*, 5013.
- (31) Stewart, J.; Wilson, D. B.; Ganem, B. *J. Am. Chem. Soc.* **1990**, *112*, 4582.
- (32) Bartlett, P. A.; Johnson, C. R. *J. Am. Chem. Soc.* **1985**, *107*, 7792.
- (33) Ganem, B. *Tetrahedron* **1978**, *34*, 3353.
- (34) Hilvert, D.; Nared, K. D. *J. Am. Chem. Soc.* **1988**, *110*, 5593.
- (35) Jackson, D. Y.; Jacobs, J. W.; Sugawara, R.; Reich, S. H.; Bartlett, P. A.; Schultz, P. G. *J. Am. Chem. Soc.* **1988**, *110*, 4841.
- (36) Hilvert, D.; Carpenter, S. H.; Nared, K. D.; Auditor, M. T. *Proc. Natl. Acad. Sci. U.S.A.* **1988**, *14*, 4953.
- (37) Acevedo, O.; Armacost, K. J. *J. Am. Chem. Soc.* **2010**, *132*, 1966.
- (38) Repasky, M. P.; Guimaraes, C. R. W.; Chandrasekhar, J.; Tirado-Rives, J.; Jorgensen, W. L. *J. Am. Chem. Soc.* **2003**, *125*, 6663.
- (39) Kincaid, J. F.; Tarbell, D. S. *J. Am. Chem. Soc.* **1939**, *61*, 3085.
- (40) Chanda, A.; Fokin, V. V. *Chem. Rev.* **2009**, *109*, 725.
- (41) Narayan, S.; Muldoon, J.; Finn, M. G.; Fokin, V. V.; Kolb, H. C.; Sharpless, K. B. *Angew. Chem., Int. Ed.* **2005**, *44*, 3275.
- (42) Ganem, B. *Angew. Chem., Int. Ed.* **1996**, *35*, 936.
- (43) Copley, S. D.; Knowles, J. R. *J. Am. Chem. Soc.* **1987**, *109*, 5008.

- (44) Guest, J. M.; Craw, J. S.; Vincent, M. A.; Hillier, I. H. *J. Chem. Soc., Perkin Trans. 2* **1997**, 2, 71.
- (45) Paton, R. S.; Mackey, J. L.; Kim, W. H.; Lee, J. H.; Danishefsky, S. J.; Houk, K. N. *J. Am. Chem. Soc.* **2010**, 132, 9335.
- (46) Ganesh, M.; Seidel, D. *J. Am. Chem. Soc.* **2008**, 130, 16464.
- (47) Huang, J.; Corey, E. J. *Org. Lett.* **2004**, 6, 5027.
- (48) Vance, R. L.; Rondan, N. G.; Houk, K. N.; Jensen, F.; Borden, W. T.; Komornicki, A.; Wimmer, E. *J. Am. Chem. Soc.* **1988**, 110, 2314.
- (49) Marti, S.; Andres, J.; Moliner, V.; Silla, E.; Tunon, I.; Bertran, J. *J. Am. Chem. Soc.* **2003**, 126, 311.
- (50) Claeysens, F.; Ranaghan, K. E.; Lawan, N.; Macrae, S. J.; Manby, F. R.; Harvey, J. N.; Mulholland, A. J. *Org. Biomol. Chem.* **2011**, 9, 1578.
- (51) Rothlisberger, D.; Khersonsky, O.; Wollacott, A. M.; Jiang, L.; Dechancie, J.; Betker, J.; Gallaher, J. L.; Althoff, E. A.; Zanghellini, A.; Dym, O.; Albeck, S.; Houk, K. N.; Tawfik, D. S.; Baker, D. *Nature* **2008**, 453, 190.
- (52) Jiang, L.; Althoff, E. A.; Clemente, F. R.; Doyle, L.; Rothlisberger, D.; Zanghellini, A.; Gallaher, J. L.; Betker, J. L.; Tanaka, F.; Barbas, C. F.; Hilvert, D.; Houk, K. N.; Stoddard, B. L.; Baker, D. *Science* **2008**, 319, 1387.
- (53) Siegel, J. B.; Zanghellini, A.; Lovick, H. M.; Kiss, G.; Lambert, A. R.; St.Clair, J. L.; Gallaher, J. L.; Hilvert, D.; Gelb, M. H.; Stoddard, B. L.; Houk, K. N.; Michael, F. E.; Baker, D. *Science* **2010**, 329, 309.
- (54) DeChancie, J.; Clemente, F. R.; Gunaydin, H.; Smith, A. J. T.; Zhang, X.; Zhao, Y.-L.; Houk, K. N. *J. Org. Chem.* **2007**, 16, 1851.
- (55) Tantillo, D. J.; Jiangang, C.; Houk, K. N. *Curr. Opin. Chem. Biol.* **1998**, 2, 743.
- (56) Ujaque, G.; Tantillo, D. J.; Hu, Y.; Houk, K. N.; Hotta, K.; Hilvert, D. *J. Comput. Chem.* **2003**, 24, 98.
- (57) Berman, H.; Henrick, K.; Nakamura, H. *Nat. Struct. Mol. Biol.* **2003**, 10, 980.
- (58) Zanghellini, A.; Jiang, L.; Wollacott, A. M.; Cheng, G.; Meiler, J.; Althoff, E. A.; R  thlisberger, D.; Baker, D. *Protein Sci.* **2006**, 15, 2785.
- (59) Das, R.; Baker, D. *Annu. Rev. Biochem.* **2008**, 77, 363.
- (60) Richter, F.; Leaver-Fay, A.; Khare, S. D.; Bjelic, S.; Baker, D. *PLoS ONE* **2011**, 6, e19230.
- (61) Zhang, X.; Houk, K. N. *Acc. Chem. Res.* **2005**, 38, 379.
- (62) Breslow, R.; Dong, S. D. *Chem. Rev.* **1998**, 98, 1997.
- (63) Cram, D. J. *Angew. Chem., Int. Ed.* **1988**, 27, 1009.
- (64) Rebek, J. *Science* **1987**, 235, 1478.
- (65) Wiester, M. J.; Ulmann, P. A.; Mirkin, C. A. *Angew. Chem., Int. Ed.* **2011**, 50, 114.
- (66) Meeuwissen, J.; Reek, J. N. H. *Nat. Chem.* **2010**, 2, 615.
- (67) Dalko, P. L.; Moisan, L. *Angew. Chem., Int. Ed.* **2001**, 40, 3726.
- (68) Hastings, C. J.; Pluth, M. D.; Bergman, R. G.; Raymond, K. N. *J. Am. Chem. Soc.* **2010**, 132, 6938.
- (69) Kheirabadi, M.; Celebi-Olcum, N.; Parker, M. F. L.; Zhao, Q.; Kiss, G.; Houk, K. N.; Schafmeister, C. E. *J. Am. Chem. Soc.* **2012**, 134, 18345.
- (70) Brown, Z. Z.; Schafmeister, C. E. *J. Am. Chem. Soc.* **2008**, 130, 14382.
- (71) Gupta, S.; Schafmeister, C. E. *J. Org. Chem.* **2009**, 74, 3652.
- (72) Brown, Z. Z.; Schafmeister, C. E. *Org. Lett.* **2010**, 12, 1436.
- (73) Sigala, P. A.; Kraut, D. A.; Caaveiro, J. M. M.; Pybus, B.; Ruben, E. A.; Ringe, D.; Petsko, G. A.; Herschlag, D. *J. Am. Chem. Soc.* **2008**, 130, 13696.
- (74) Schwans, J. P.; Sunden, F.; Gonzalez, A.; Tsai, Y.; Herschlag, D. *J. Am. Chem. Soc.* **2011**, 133, 20052.
- (75) Gerlt, J. A.; Gassman, P. G. *Biochemistry* **1993**, 32, 11943.
- (76) Gerlt, J. A.; Gassman, P. G. *J. Am. Chem. Soc.* **1993**, 115, 11552.
- (77) Guthrie, J. P. *Chem. Biol.* **1996**, 3, 163.
- (78) Warshel, A.; Papazyan, A.; Kollman, P. A.; Cleland, W. W.; Kreevoy, M. M.; Frey, P. A. *Science* **1995**, 269, 102.
- (79) Cornell, W. D.; Cieplak, P.; Bayly, C. I.; Gould, I. R.; Merz, K. M.; Ferguson, D. M.; Spellmeyer, D. C.; Fox, T.; Caldwell, J. W.; Kollman, P. A. *J. Am. Chem. Soc.* **1995**, 117, 5179.
- (80) Chakrabarti, S.; Parker, M. F. L.; Morgan, C. W.; Schafmeister, C. E.; Waldeck, D. H. *J. Am. Chem. Soc.* **2009**, 131, 2044.
- (81) Brown, Z. Z.; Alleva, J.; Schafmeister, C. E. *Pept. Sci.* **2011**, 96, 578.
- (82) Schafmeister, C. E.; Brown, Z. Z.; Gupta, S. *Acc. Chem. Res.* **2008**, 41, 1387.
- (83) Palacin, S.; Chin, D. N.; Simanek, E. E.; MacDonald, J. C.; Whitesides, G. M. *J. Am. Chem. Soc.* **1997**, 119, 11807.
- (84) Maestro *Ligprep, Macromodel, Glide and QikProp*; Schrodinger, LLC; New York, NY, 2011; <http://www.schrodinger.com>.
- (85) Jorgensen, W. L.; Maxwell, D. S.; Tirado-Rives, J. *J. Am. Chem. Soc.* **1996**, 118, 11225.
- (86) Zhao, Y.; Truhlar, D. G. *Acc. Chem. Res.* **2008**, 41, 157.
- (87) Hehre, W. J.; Ditchfield, R.; Pople, J. A. *J. Chem. Phys.* **1972**, 56, 2257.
- (88) Hariharan, P. C.; Pople, J. A. *Theor. Chim. Acta* **1973**, 28, 213.
- (89) Barone, V.; Cossi, M. *J. Phys. Chem. A* **1998**, 102, 1995.
- (90) Case, D. A.; Darden, T. A.; Cheatham, T. E.; Simmerling, C. L.; Wang, J.; Duke, R. E.; Luo, R.; Crowley, M.; Walker, R. C.; Zhang, W.; Merz, K. M.; Wang, B.; Hayik, S.; Roitberg, A.; Seabra, G.; Kolossv  ry, I.; Wong, K. F.; Paesani, F.; Vanicek, J.; Wu, X.; Brozell, S. R.; Steinbrecher, T.; Gohlke, H.; Yang, L.; Tan, C.; Mongan, J.; Hornak, V.; Cui, G.; Mathews, D. H.; Seetin, M. G.; Sagui, C.; Babin, V.; Kollman, P. A. *AMBER 11*; University of California, San Francisco, 2011.
- (91) Waterhous, D. V.; Muccio, D. D. *Magn. Reson. Chem.* **1990**, 28, 223.

#### ■ NOTE ADDED AFTER ASAP PUBLICATION

Figure 2 has been updated. The revised version was re-posted on March 3, 2014.